JEE Journal of Ecological Engineering

Journal of Ecological Engineering, 2025, 26(1), 121–136
https://doi.org/10.12911/22998993/195428
ISSN 2299–8993, License CC-BY 4.0

Received: 2024.10.17
Accepted: 2024.11.16
Published: 2024.12.01

The pore water pressure changes on forested slopes in tropical humid climate area

Hendrayanto[1*], Yulia Amirul Fata[2,3*], Muhamad Askari[4], Erizal[5], Suria Darma Tarigan[6], Ery Suhartanto[7]

[1] Forest Management Department, IPB University, Jl. Dramaga, Bogor, Indonesia
[2] Soil Science Department, Brawijaya University, Jl. Veteran, Malang, Indonesia
[3] Graduate Student of Forest Management Department, IPB University, Jl. Dramaga, Bogor, Indonesia
[4] Faculty of Sustainable Agriculture, Universiti Malaysia Sabah, Malaysia, Locked Bag No. 3, 90509 Sandakan, Sabah, Malaysia
[5] Civil and Environmental Engineering Department, IPB University, Jl. Dramaga, Bogor, Indonesia
[6] Soil and Land Resources Science Department, IPB University, Jl. Dramaga, Bogor, Indonesia
[7] Water Resources Engineering Department, Brawijaya University, Jl. Veteran, Malang, Indonesia
* Corresponding author's e-mail: hendrayanto@apps.ipb.ac.id

ABSTRACT

This study investigates the pore water pressure and water content on a forested slope, focusing on the impact of canopy interception across various rainfall intensities. The study was performed on slopes in the Sukajaya Sub District of West Bogor, West Java, Indonesia, a region that encountered landslides in 2020. Soil hydraulic characteristics, soil textures, saturated water content, and soil moisture content at different pressures, were assessed at different slope locations and depths. The pore water pressure and water content change were simulated using the one-dimensional uniform (equilibrium) finite element model of water movement using the modified Richards and were executed with the HYDRUS 1D model across six scenarios of a combination of three rainfall events at two initial conditions of water content, contrasting bare and vegetated slopes of *Maesopsis eminii*, which exhibited 35% canopy interception. Findings demonstrate that bare soil attains saturation more rapidly, resulting in elevated pore water pressure and increased susceptibility to slope instability. Conversely, vegetated slopes have delayed saturation owing to canopy interception, which diminishes the volume of rainfall that reaches the soil. The results highlight the crucial function of vegetation in preserving slope stability by regulating soil water pressure and water content, particularly during intense rainfall events. This research enhances comprehension of how vegetated areas might reduce landslide hazards in high-rainfall environments.

Keywords: pore water pressure, canopy interception, soil hydraulic characteristics, HYDRUS 1D, slope stability, forested slopes.

INTRODUCTION

Soil pore water pressure (PWP) is a hydrostatic pressure generated by water contained in the cavities between the soil grains or the gaps between the rocks. The groundwater pressure under the groundwater table (phreatic zone) is of positive value, and above the groundwater table (vadose zone) is worth negative as tension, suction, or matric pressure. When water gets into the soil (infiltrate), the water fills the cavities of the soil or the crevices of the rocks. It exerts pressure on the soil grains surrounding the soil, and when the cavity of the water-saturated soil cavity creates positive pore water pressure. An increased value of PWP indicates the saturation of the soil. As the saturation increases, the initially negative PWP value will increase to a positive value. The gradual increase in these values as rainfall is applied affects the strength and soil instability [Ibrahim et al., 2013; Maturidi et al., 2021].

The PWP in the soil affects slope stability. As PWP increases, soil strength will decrease and the chance of slope failure will increase

[Terzaghi, 1923; Wu et al., 1979]. Recent studies demonstrate that elevated pore water pressure might diminish soil strength, thereby increasing the risk of slope failure mainly triggered by rainwater infiltration [Elfadil 2018; Tian et al., 2022] and groundwater fluctuation [Hemid et al., 2021]. PWP also affects the water flow in the soil and the availability of water to plants, the smaller the soil water pressure (matric pressure increases) the more difficult the water flows and the more difficult it is to be utilized by plants [Couvreur et al., 2014; Kharel et al., 2023].

The relationship between soil moisture content (*θ)* and PWP, matric pressure (*φ*) is commonly described in the form of a soil water retention curve (SWRC). It is influenced by soil hydraulics properties that reflect the structure of the soil porous system, which consists of pores of different geometry, size [Jabro and Stevens, 2022], and connectivity [Dexter, 1988; Kuti'lek and Nielsen, 1994]. These properties also reflect soil texture, surface and subsurface compactness, soil biota, salinity and sodicity, surface crust and sealing, and soil temperature [El-Ghany et al., 2010; Dlapa et al., 2020]. The nature of soil hydraulics also affects the function of soil hydraulic conductivity (*K*) [Brook and Corey, 1964; Mualem, 1976] against φ - θ [Van Genuchten, 1980; Kosugi, 1996].

The soil hydraulics properties related to SWRC and *K* vary by space and time [Hendrickx et al., 2023; Proteau et al., 2023]. Forested soils show large spatial variations of SWRC and *K* [Bonell, 1993; Buttle and House, 1997]. Large spatial variation is due to the large number of macropores in forested soils due to faunal activity and high root density [Noguchi et al., 1997; Proteau et al., 2023]. The presence of macropores in soil causes the spatial distribution of soil pore radius to vary greatly in forest soil [Kosugi, 1996; Kosugi, 1997]. In forested soils, matric pressure is positively correlated with the median pore radius, generally small at the top and top of the slope and larger at the middle and foot of the slope, but at the top surface of the slope, the matric pressure is greater than the subsurface, which is thought to be due to the formation of a good crumb structure in the surface layer of forested soil [Hendrayanto et al., 2000; Guan et al., 2023]. Saturated soil hydraulic conductivity is generally small at the top and top of the slope, and larger at the middle and foot of the slope, The amount of saturated hydraulic conductivity is related to the magnitude of matric pressure [Hendrayanto et al., 1999].

The nature of soil hydraulics properties, especially in the surface soil layer, can change due to land use activities [Yu et al., 2015; Agbai and Kosuowei 2022], including changes in forest type [Virano-Riquelme et al., 2022], plant type, the intensity of change [Asdak et al., 1998; Móricz et al., 2012], and land management [Podhrázská et al., 2021]. Land use also affects the net rainfall that reaches the surface of mineral soils [Dietz et al., 2016] through the process of interception [Sidle and Ziegler, 2017; Zhong et al., 2020]. The magnitude of interception varies depending on vegetation characteristics [Gonzalez-Ollauri and Mickovski, 2017; Suryatmojo and Imron, 2017]. Type vegetation also affects the special distribution of net rainfall reaching the mineral soils [Prado Hernández et al., 2023; Li et al., 2023]. Rashid et al., [2015] show that stemflow rates of oil palm are much higher than the throughfall rates, causing much higher local infiltration rates near the trees stem areas than in areas away from the trees. The streamflow-induced water produces litter marks that can be used for area infiltration estimation [Rashid and Askari, 2014]. The aerial part of a 10-year-old willow intercepted rainfall up to 26.73% and further concentrated around the stem at 10.78% [Gonzalez-Ollauri and Mickovski, 2017].

The results of the research explained above show that the amount of precipitation intercepted by vegetation, and the nature of soil hydraulics vary according to space and time so that the rainfall-vegetation-soil interaction and the interaction response of these three factors to PWP are site-specific. Research on pore water changes as a result of rainfall, land use, and hydraulics properties in areas that have experienced landslides has not been widely conducted, while knowledge about changes in PWP due to rainfall intensity and duration in an area, especially on forested slopes is needed in explaining the occurrence of landslides in the region. This study aims to analyze the changes in soil PWP on slopes as the effect of canopy interception in response to different rainfall intensities in areas that have experienced landslides.

METHODOLOGY

Research site

The research was carried out on bare hill slopes, and vegetated hill slopes of *Maesopsis eminii* stands in Sukajaya Sub District, Bogor

District, West Java Province, Indonesia (Fig. 1). Sukajaya sub-district was the area that experienced a landslide on January 1, 2020.

Changes in pore water pressure analysis

The pore water pressure (PWP) change was simulated using the one-dimensional uniform (equilibrium) finite element model of water movement using the modified Richards Equation 1. The air phase is considered to have a negligible impact on the liquid flow process, and thermal gradients do not affect water flow [Simunek et al., 2013].

$$\frac{\partial \theta}{\partial t} = \frac{\partial}{\partial z}\left[K(\varphi)\left(\frac{\partial \varphi}{\partial z} + Cos\ \alpha\right)\right] + S \tag{1}$$

where: φ represents the water pressure head [cm], θ denotes the volumetric water content (cm^3/cm^3), t signifies time (day), z indicates soil depth (cm), S refers to the sink term (cm^3/cm^3/day), α describes the slope flow direction relative to the vertical axis (where $\alpha = 0°$ corresponds to vertical flow, 90° to horizontal flow, and $0° < \alpha < 90°$ to inclined flow), and $K(\varphi)$ is the function of unsaturated hydraulic conductivity (cm/day) as defined by Equation 2:

$$K(\varphi,z) = Ks(z)\ Kr(\varphi,z) \tag{2}$$

where: Kr signifies the relative hydraulic conductivity and Ks indicates the saturated hydraulic conductivity (cm/day).

The unsaturated soil hydraulic properties, $\theta(\varphi)$ and $K(\varphi)$, in Equation 1 utilize the soil-hydraulic functions proposed by van Genuchten [1980], who employed Mualem [1976] statistical pore-size distribution model to derive a predictive equation for the unsaturated hydraulic conductivity function based on soil water retention parameters. Van Genuchten [1980] presented the equations for $\theta(\varphi)$ and $K(\varphi)$ are given by (Equation 3 and Equation 4).

$$\theta(\varphi) = \begin{cases} \theta_r + \frac{\theta_s - \theta_r}{[1+|\alpha\varphi|^n]^m}, \varphi < 0 \\ \theta_s, \varphi \geq 0 \end{cases} \tag{3}$$

$$K(\varphi) = K_s S_e^l [1 - (1 - S_e^{l/m})]^2 \tag{4}$$

where:

$$m = 1\text{-}1/n,\ n > 1 \tag{5}$$

The three of five independent parameters of θr, θs, and Ks used the measure values of the samples, while the values of α and n used the result of fitting model of Equation 3 and measured soil water retention curve. The parameter l (pore connectivity) in Equation 4 is estimated to be about

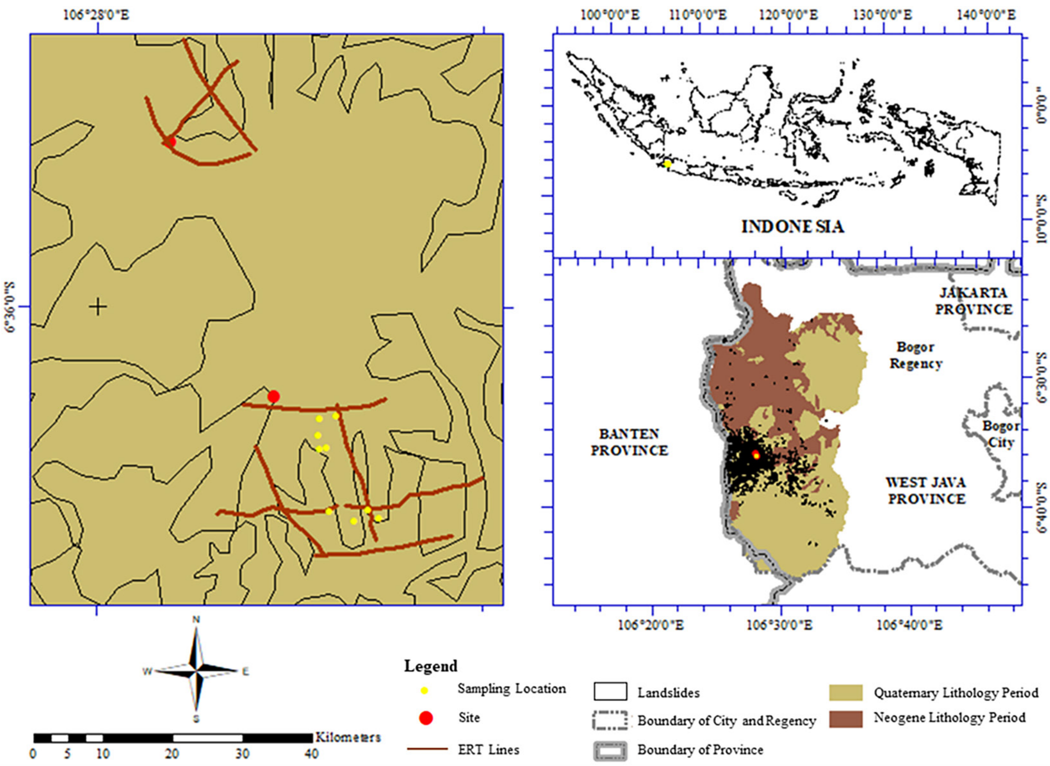

Figure 1. Location of electrical resistivity tomography (ERT) and interception measurement [Fata et al., 2021; Fata et al 2023]

0.5 [Mualem, 1976] as an average for many soils. The *Se* is effective saturation.

The fitting parameter used the non-linear least squares method, where the best fitting values are when the residual sum squares were minimum. The optimization procedure used solver commands in Microsoft Excel software [Anlauf, 2014]. The numerical solving equations used the HYDRUS 1D program [Tárník and Igaz, 2020] in HYDRUS 1D package software 4.17.

Soil profile, initial, and boundary conditions

The soil profile as flow domain in each point of simulation (in the crest, middle, and foot slopes) is set similarly to the field condition, where the solum (z) is 600 cm (ERT Survey, Fata et al., 2021], consists of two layers (1st layer is < 50 cm and the 2nd is > 50–600 cm). Soil hydraulic properties (θs, θs, Ks) of each layer are set as equal to the laboratory soil sample analysis, and optimized parameters of α and n of van Genuchten [1980] soil-hydraulic model.

The system-dependent type boundary condition is set, where the soil surface is exposed to atmospheric conditions (atmospheric boundary condition with surface runoff) and deep drainage at the bottom. The initial condition (IC) is set equal to the θ at pF1, and pF2 at the surface of each layer (at the surface and -50 cm depth), and θs at the bottom.

The rainfall as the input for simulation water flow applied measured and simulated daily rainfall to figure the rainfall when no landslides and landslides occurred in the location area, that was 200 mm/day. The rainfall simulation important to model the rainfall threshold for landslide susceptibility analysis [Salee et al., 2022].

Simulation of pore water pressure changes scenario

Six scenarios were applied under defined soil profile, initial and boundary conditions, those are LU1-RF1, LU1-RF2, LU1-RF3, LU2-RF1, LU2-RF2, LU2-RF3 scenarios (Table 1), where:

LU1 and LU2 are LU1 is bare land with no canopy interception and LU2 is Land with 35% canopy interception (*Maesopsis eminii* stand) [Fata et al., 2023].

RF1, RF2, and RF3 are three different seven days of consecutive daily rainfalls that were selected from measured daily rainfalls. The amounts of 7 day rainfalls were > 200 mm as indicated in Table 1. The RF1, RF2, and RF3 scenarios used 7 days of cumulative rainfall > 200 mm/day and were based on the intensity of rainfall at the time of a major landslide occurrence at the study site. The rainfall of 200 mm/day at the time the landslide occurred was preceded by a lower rainfall intensity of < 200 mm/day.

RESULTS AND DISCUSSION

Soil hydraulic properties

Soil hydraulic properties based on laboratory measurements of soil samples taken from crest, middle, and foot slopes at surface layer (I) and lower layer (II) are presented in Table 2 and Table 3. The optimized parameters of the Van Genuchten model are presented in Table 4.

Graphically, the soil-water retention of the Van Genuchten model is presented in Figure 2, and the function of unsaturated hydraulic conductivity and soil-water retention (φ) is presented in Figure 3.

Table 1. LU-RF Scenarios in soil pore water pressure change simulations

Days	LU1			LU2		
	RF1 (mm)	RF2 (mm)	RF3 (mm)	RF1 (mm)	RF2 (mm)	RF3 (mm)
Day 1	9.5	121.0	14.8	9.5	121.0	14.8
Day 2	25.0	95.6	11.2	25.0	95.6	11.2
Day 3	121.0	0.0	13.8	121.0	0.0	13.8
Day 4	95.6	21.0	21.0	95.6	21.0	21.0
Day 5	0.0	20.0	46.6	0.0	20.0	46.6
Day 6	21.0	0.0	8.4	21.0	0.0	8.4
Day 7	20.0	7.4	88.1	20.0	7.4	88.1
Cumulative 7 days Rainfall (mm)	282.6	265.0	203.9	282.6	265.0	203.9

Note: LU is land use and RF is rainfall.

Table 2. Physical soil properties at crest, middle, and foot slopes at the soil surface (I, 0–50 cm) and lower surface (II, > 51 cm)

Parameter	Unit	Crest		Middle		Foot	
		I	II	I	II	I	II
a. Soil texture							
Sand	(%)	4.6	8.6	3.8	2.94	5.1	6.2
Silt	(%)	46.2	30.8	28.1	29.89	14.4	32.3
Clay	(%)	49.2	60.6	68.1	67.2	80.6	61.5
b. Bulk density	(g/cc)	0.66	0.63	0.68	0.69	0.70	0.76
c. Porosity	(%)	66.0	70.2	65.6	67.1	64.3	63.6
d. Saturated water content (*qs*)	(%)	64.7	68.8	64.3	65.8	63.0	62.3

Table 3. Soil water retention and water content at crest, middle, and foot slopes at soil surface (I, 0–50 cm) and lower surface (II, > 50 cm)

Retention (pF)	Crest		Middle		Foot	
	I	II	I	II	I	II
	Water Content (%)					
1	54.60	63.85	57.80	62.00	50.30	54.80
2	50.15	55.95	49.70	50.60	45.00	48.80
2.4	45.40	49.15	41.55	45.85	39.20	45.00
4.2	22.50	22.65	23.85	23.95	21.75	23.10

Table 4. Optimized van Genuchten model parameters

Parameter	Unit	Crest		Middle		Foot	
		I	II	I	II	I	II
$q_{observed}$	(cm^3/cm^3)	0.66	0.702	0.6565	0.6710	0.6425	0.6355
qs	(cm^3/cm^3)	0.66	0.702	0.6565	0.6710	0.6425	0.6355
qr	(cm^3/cm^3)	0.2250	0.2265	0.2385	0.2395	0.2175	0.2310
a	(1/cm)	0.0345	0.0088	0.0239	0.0151	0.1321	0.0221
n	–	1.6388	2.0169	1.8335	1.9026	1.5415	1.7277
m	–	0.3898	0.5042	0.4546	0.4744	0.3513	0.4212
Ks	(cm/day)	131.40	100.92	133.56	112.32	94.92	171.84

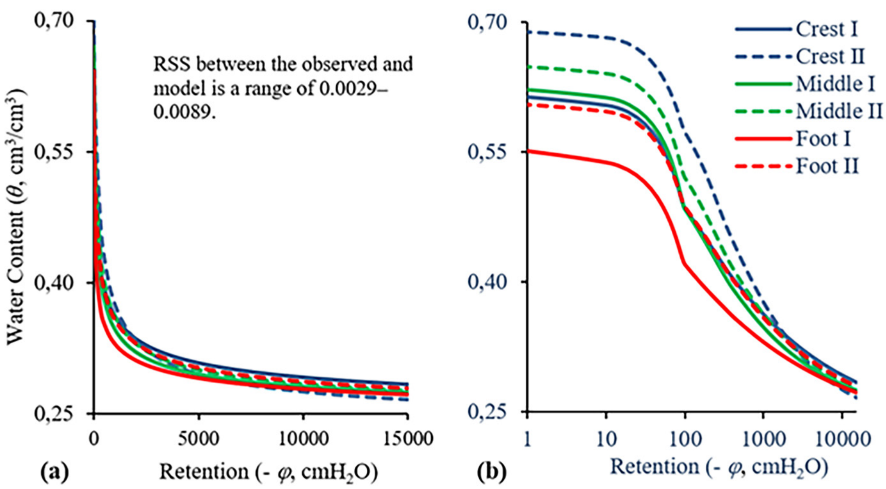

Figure 2. Soil-water retention curves of van Genuchten model: a) linear scale, b) logarithmic scale

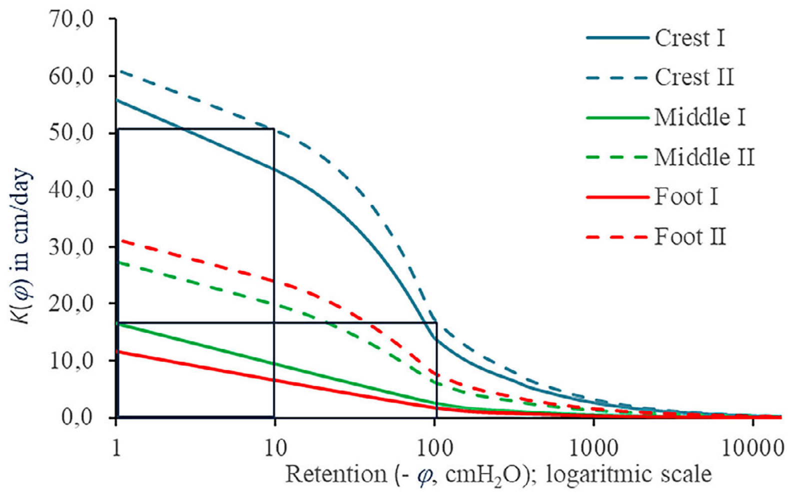

Figure 3. Unsaturated hydraulic conductivity (K) and retention (*j*) of the Van Genuchten model

The soil texture of the slope is silt-clay to clay, where the clay content is increased to foot direction and deeper layer. The bulk density also has a similar trend, which is higher in the foot slope direction and deeper layer, while the porosity tends to decrease in the foot slope direction and lower layers. The θs relate to the soil porosity, that is higher porosity has higher θs.

Figure 2 shows that the θ at the same retention is higher at lower soil layers and lower to foot slope direction, and at the retention of around -100 cmH_2O (pF2), the θ at surface layers of Crest and lower layer of foot slope are almost the same. The θ changes from near saturation (pF1) to field capacity (at pF2) are Middle I > Middle II > Crest I > Foot I > Foot II > Crest II, and the θ change from field capacity to wilting point (pF4.2) are Crest II > Middle I > Middle II > Foot II > Foot II > Crest I > Foot II.

Those soil θ and retention relations cause the $K(\varphi)$ to be higher in lower layers (> 50 cm) means that the unsaturated hydraulic conductivity of lower layers is higher than surface layers (< 50 cm) as shown in Figure 3. The $K(\varphi)$ at the same layers of Crest > Middle > Foot Slopes except for Foot Slope I is > Middle I. The differences between $K(\varphi)$ at the surface and lower layers are higher at low φ and become smaller when φ becomes higher. The highest difference occurs in the Foot Slope, while the smallest difference occurs in the Crest Slope.

Pore water pressure changes

Pore water pressure change in bare land slope

The PWP and θ changes on the bare land slope at the crest, middle, and foot slope as their response to rainfall (RF1) when the initial condition (IC) is set up as θ at pF1 (10 cm H_2O) are presented in Figure 4. The black solid line shows the IC.

Applying low rainfall intensity in the 1st and 2nd days of 9,5 and 25 mm/day respectively decreases the θ and increases PWP (higher negative pressure) at the surface layers (0 to -150 cm depth) of Crest, Middle, and Foot Slopes. The decreasing of θ on the 1st and 2nd days at surface layers of Crest and Foot Slopes are higher than Middle Slope, and smaller at deeper layers up to -150 cm. The PWP and θ changes in the surface layers of the foot slope are less compared to the PWP and θ changes in the crest and middle slopes. The PWP and θ at layers -200 cm and deeper have already reached saturation conditions (PWP = 0) on the 1st and 2nd days. The θ continuing increase as the rainfall intensity increases on the 3rd and 4th days, PWP is closer to zero, and the surface layers of the Crest and Middle Slopes reach near saturation conditions on the 4th. However, the surface layers at Foot Slopes do not reach saturation conditions until 7 days of simulation.

The PWP and θ at layer -50 cm on the 1st and 2nd days were relatively constant (do not change, equal to IC). With the rain continuing, on the 3rd day and the next days, in the layer of -150 cm and deeper, it has reached saturation. In contrast, the soil saturation reaching the soil surface only occurs on the 4th day and afterward, except in the Foot Slope, the soil saturation only reaches the -150 cm layer, not reaching the soil surface.

When the rainfall intensities are higher on the 1st and 2nd days at 121.0 and 95.6 mm/day respectively (RF2), the temporal and vertical distribution of PWP and θ changes are different as shown

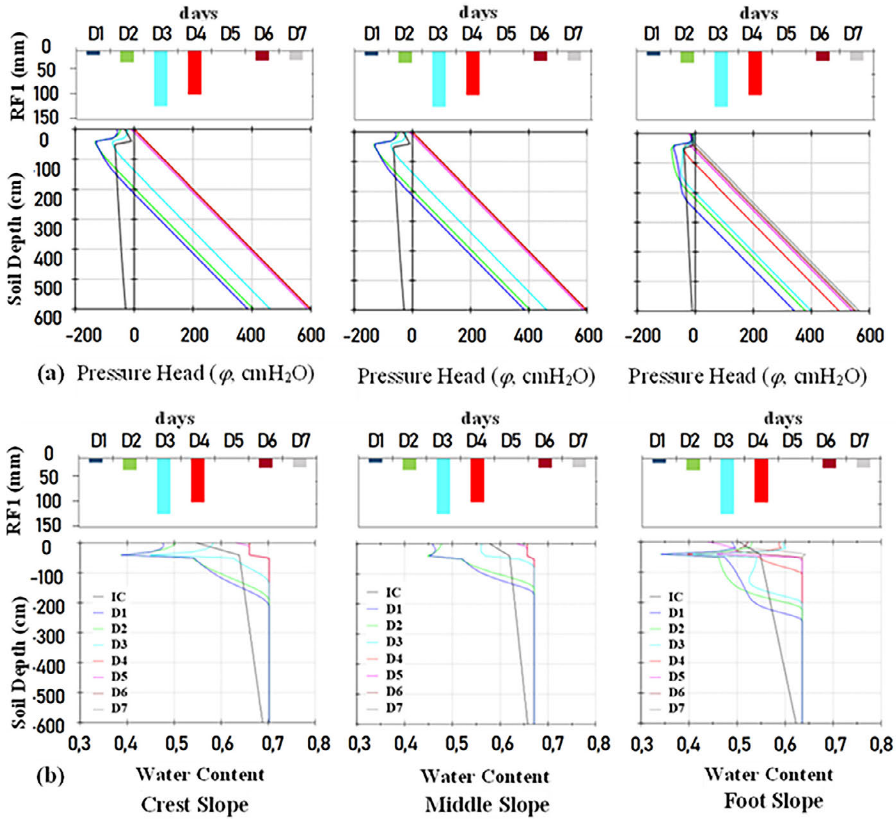

Figure 4. Temporal and vertical distribution of (a) pore water pressure, and (b) water content at bare land slope with initial condition of water content at pF1 and rainfall of RF1

in Figure 5. The saturated condition at surface layers of 0 to -50 cm is reached faster on the 2nd day at the Crest Slope and the Middle Slope. In contrast, at the foot slope, the saturated condition just reached at -120 cm layer on the same day, and saturation condition at layers up to -50 cm was reached on the 5th day.

Low daily rainfall of < 50 mm during 6 days of consecutive rainfall, and 88.1 mm on the 7th day (cumulative 7 days rain = 203.1 mm; RF3), do not cause saturation conditions at surface layers as shown in Figure 6. Saturation conditions only reach the depth up to -50 cm of the Crest and Middle Slopes and up to -150 cm depth in the Foot Slope.

Dryer IC of θ at pF2 (100 cmH_2O) the rainfall of RF1 and RF2 do not cause saturation conditions at surface layers (> -50 cm). The saturation condition only reaches deeper layers of < -200 cm (up to 200 cm below soil surface) and up to 250 cm below layers, when rainfall is RF3 as shown in Figures 7–9.

The changes of PWP and θ of surface and deeper layers at the Crest, Middle, and Foot Slopes relate to the characteristics of soil water retention $\theta(\varphi)$ and unsaturated hydraulic conductivity $K(\varphi)$. The $K(\varphi)$ is higher at surface layers than deeper layers at pF1 and higher than the rainfall intensity on the 1st and 2nd days. The infiltration rate at surface layers is higher than rainfall intensity. The rainfall intensity of 9,5 and 25 mm/day is less than $K(\varphi)$ of > 50 mm/day. The rainfall is not enough to increase the soil moisture content in the surface layers, even rain and initial soil moisture content are infiltrated into the deeper layers causing the soil moisture content at surface layers to decrease, smaller than the initial soil moisture content. The intensity of daily rainfall of > 120 cm had more effect on the change in PWP and θ than to the cumulative 7 days rainfall of 203 mm.

Pore water pressure change on forested land slope

The direct effect of canopy interception of the *Maesopsis eminii* forests is to reduce the amount of rainfall that reaches the mineral soil surface by 35% [Fata et al., 2023]. Reductions in the amount of rainfall by 35% affect the time at which soil saturation conditions are achieved, as presented in Figure 10–15. Figures 10–15 show the temporal and vertical changes of PWP and soil water content as the effect of canopy interception

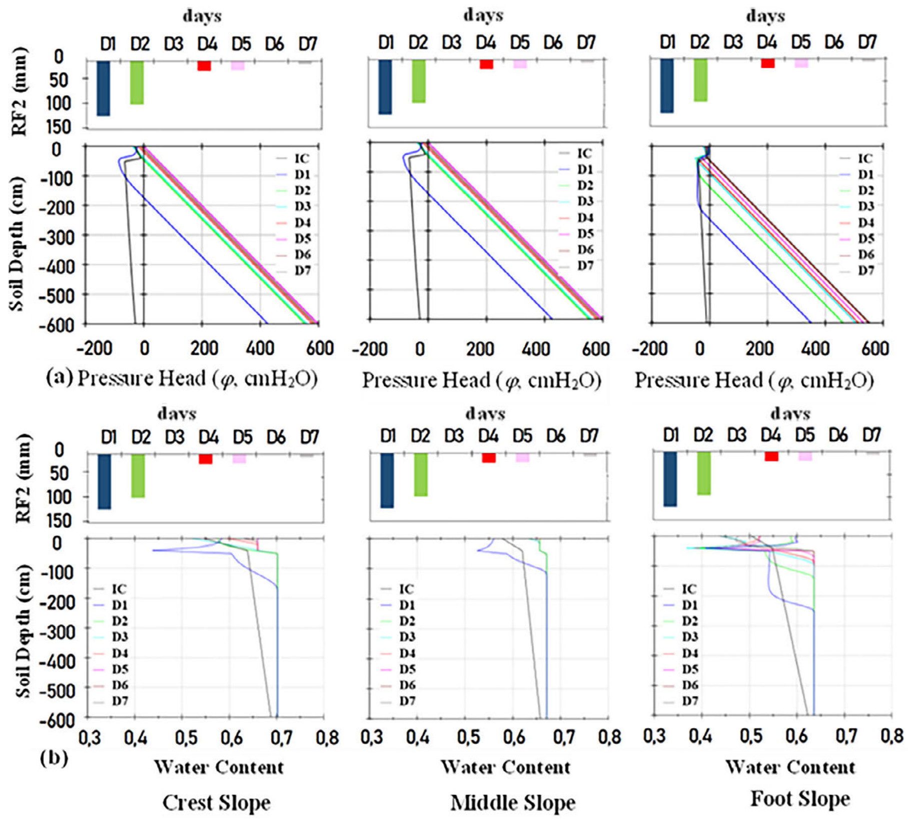

Figure 5. Temporal and vertical distribution of (a) pores water pressure, and (b) water content at bare land slope with initial condition of water content at pF1 and rainfall of RF2

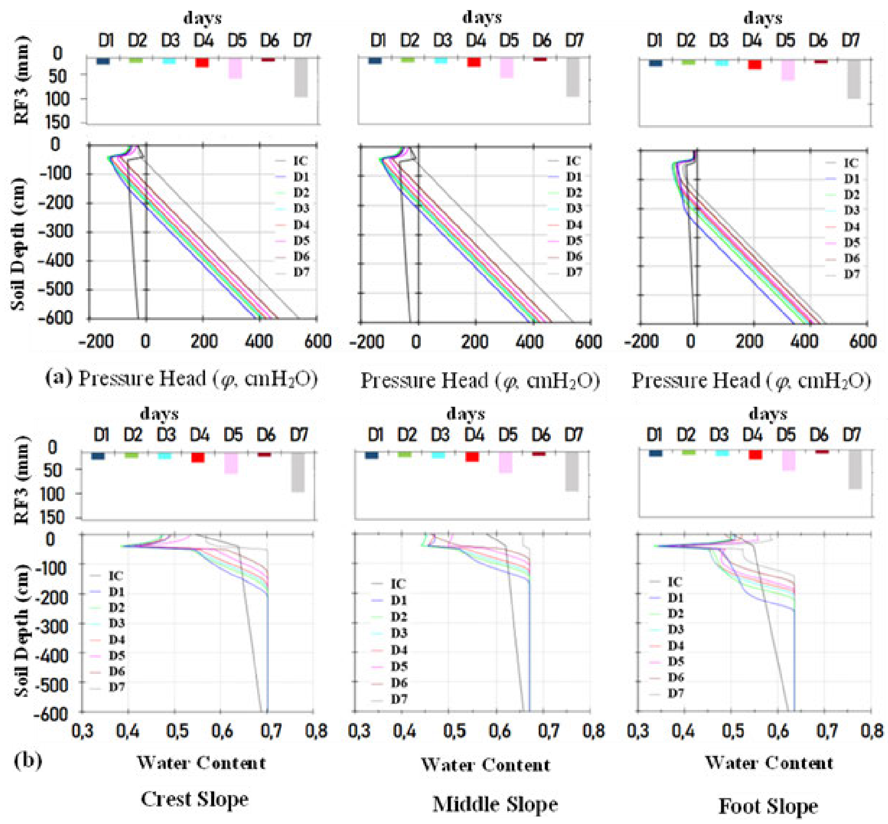

Figure 6. Temporal and vertical distribution of (a) pores water pressure, and (b) water content at bare land slope with initial condition of water content at pF1 and rainfall of RF3

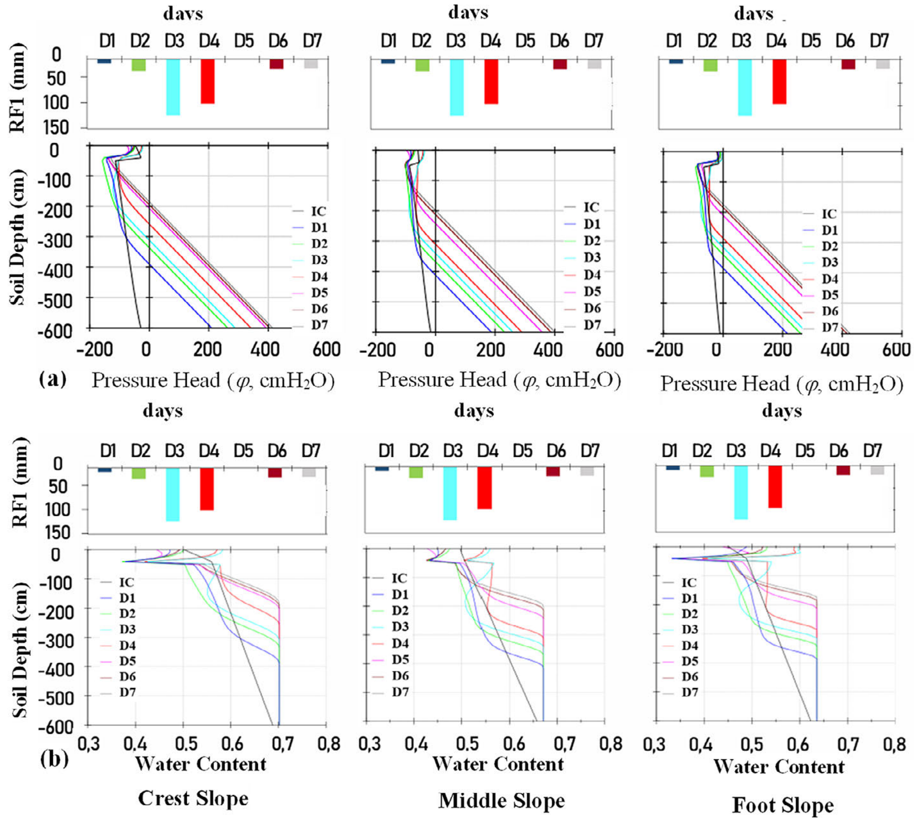

Figure 7. Temporal and vertical distribution of (a) pore water pressure, and (b) water content at bare land slope with initial condition of water content at pF 2 and rainfall of RF1

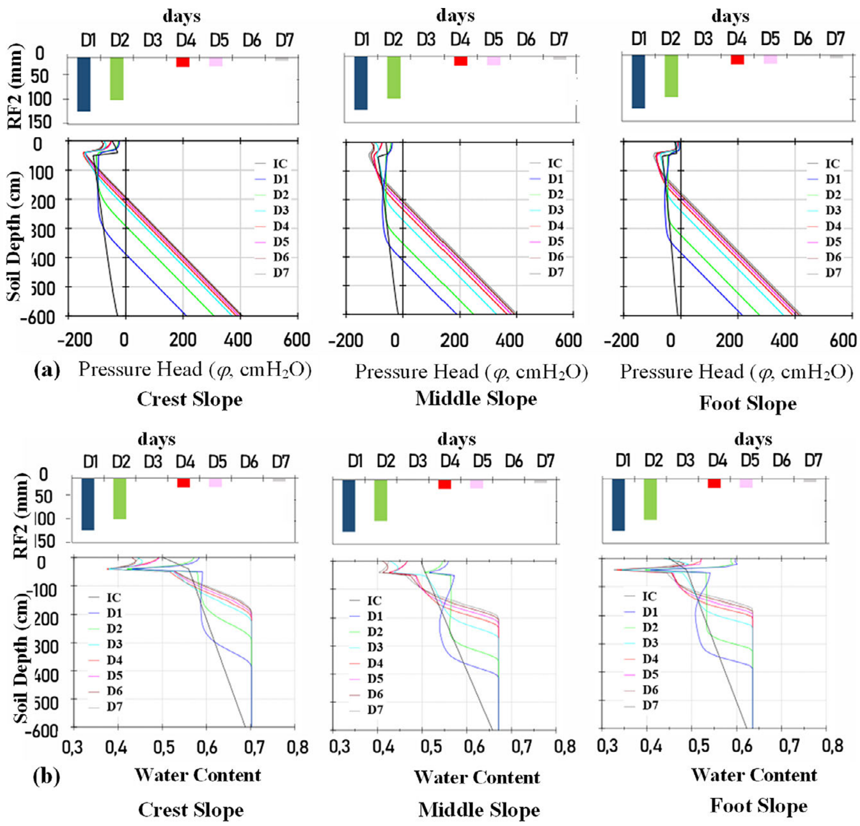

Figure 8. Temporal and vertical distribution of (a) pore water pressure, and (b) water content at bare land slope with initial condition of water content at pF2 and rainfall of RF2

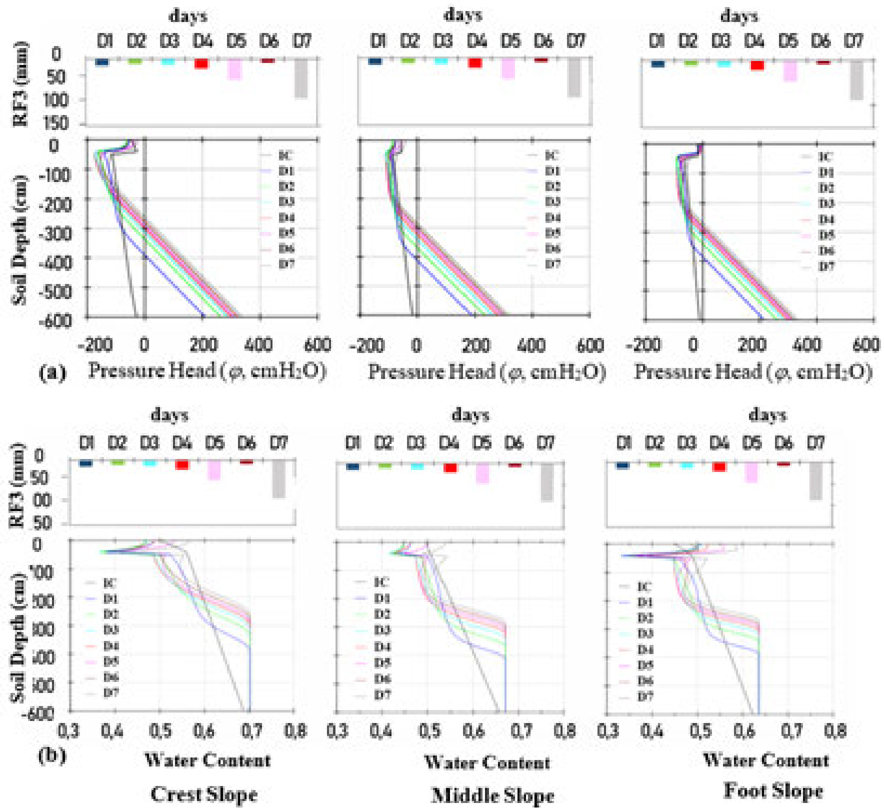

Figure 9. Temporal and vertical distribution of (a) pore water pressure, and (b) water content at bare land slope with initial condition of water content at pF2 and rainfall of RF3

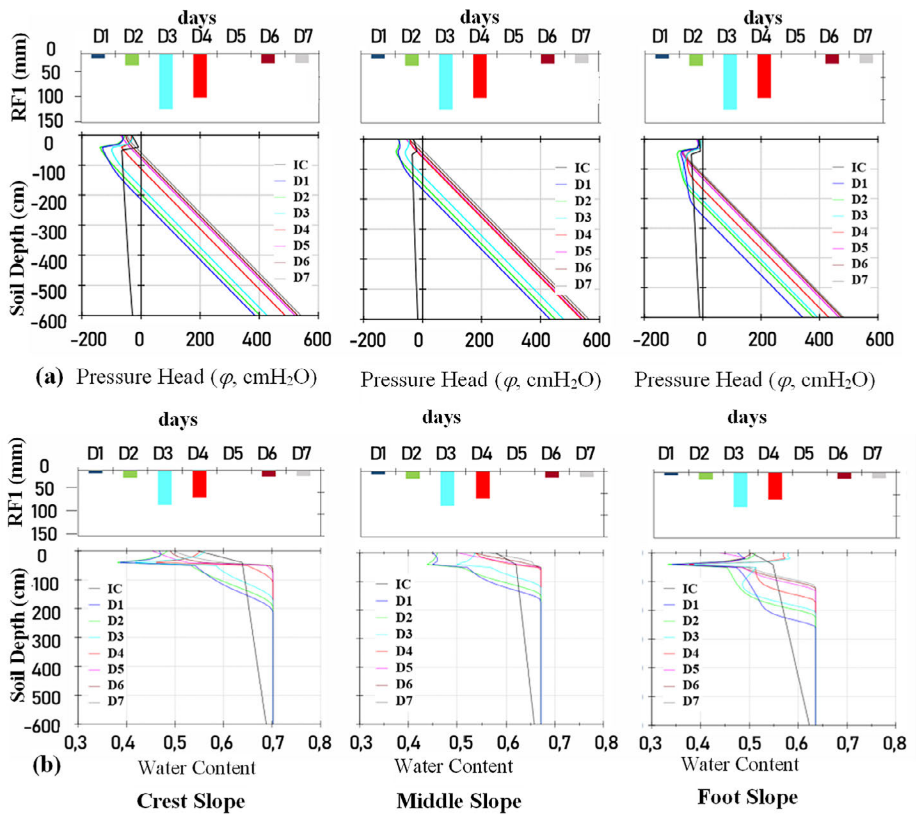

Figure 10. Temporal and vertical distribution of (a) pore water pressure, and (b) water content at vegetated slope of *Maesopsis eminii* with initial condition pF1 and rainfall of RF1

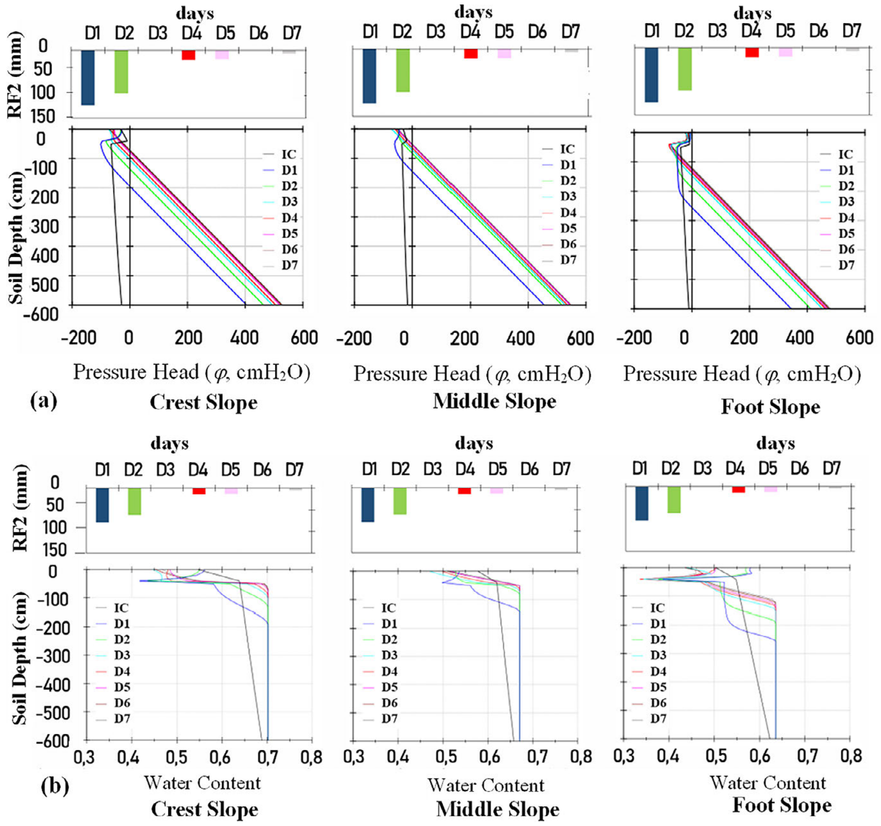

Figure 11. Temporal and vertical distribution of (a) pore water pressure, and (b) water content at vegetated slope of *Maesopsis eminii* with initial condition pF1 and rainfall of RF2

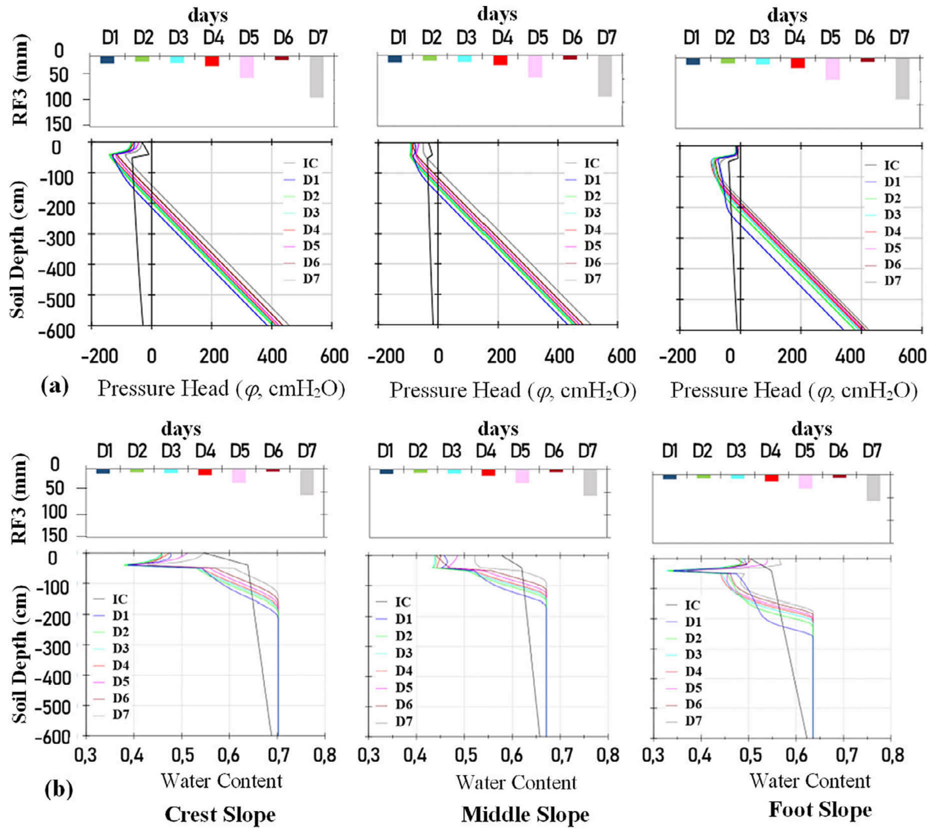

Figure 12. Temporal and vertical distribution of (a) pore water pressure, and (b) water content at vegetated slope of *Maesopsis eminii* with initial condition pF1 and rainfall of RF3

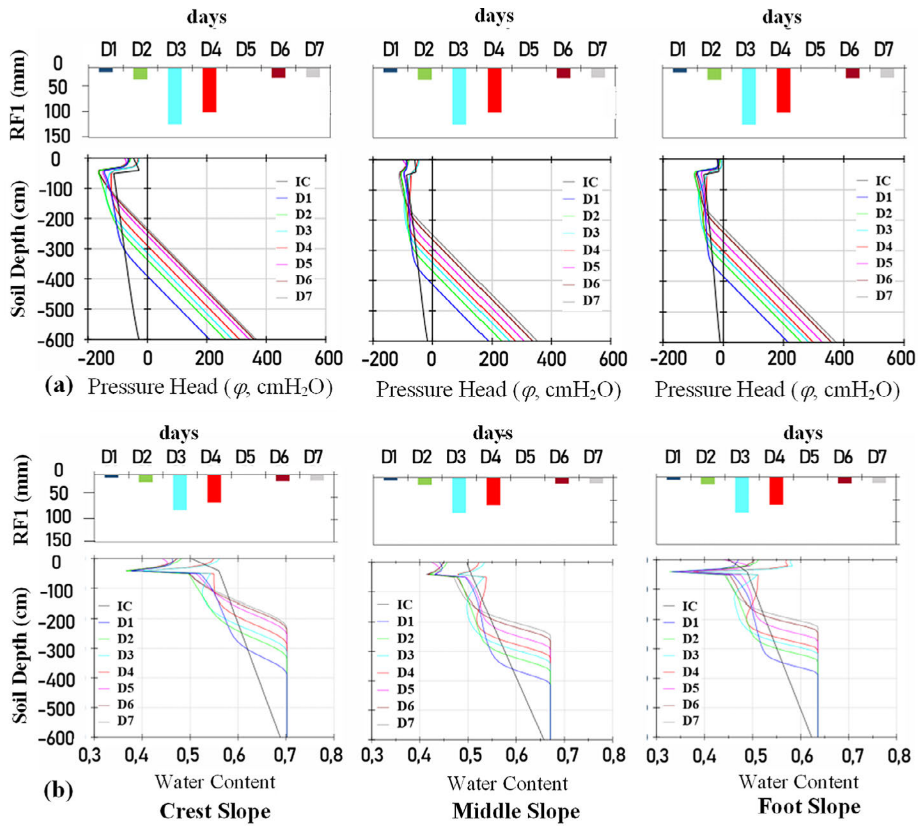

Figure 13. Temporal and vertical distribution of (a) pore water pressure, and (b) water content at vegetated slope of *Maesopsis eminii* with initial condition pF2 and rainfall of RF1

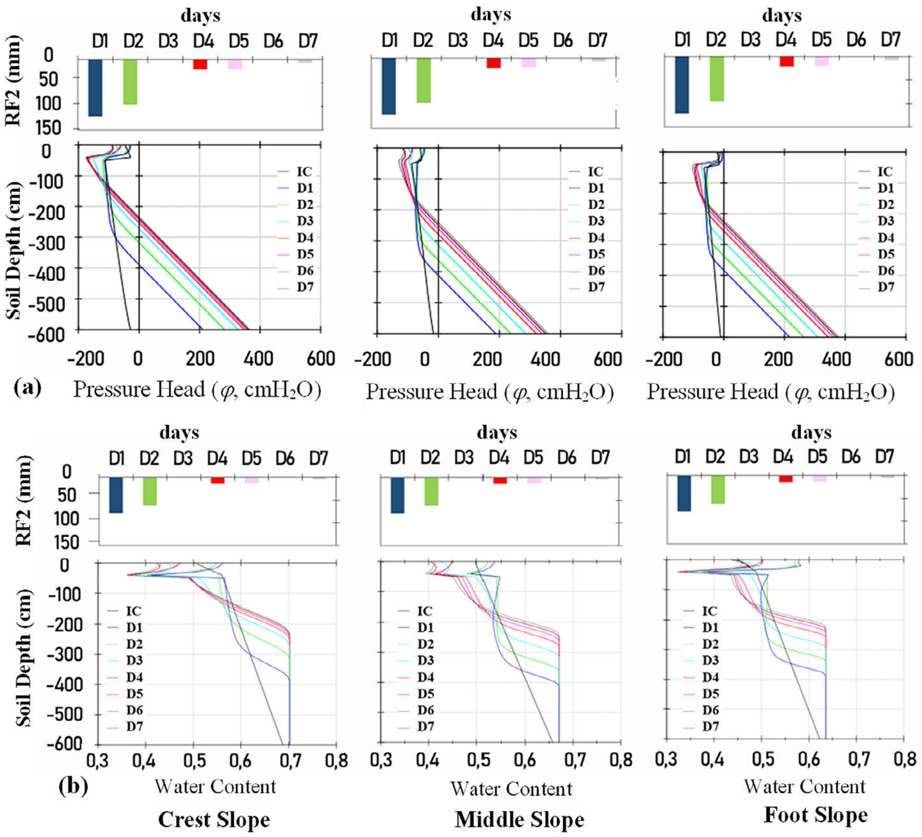

Figure 14. Temporal and vertical distribution of (a) pore water pressure, and (b) water content at vegetated slope of *Maesopsis eminii* with initial condition pF2 and rainfall of RF2

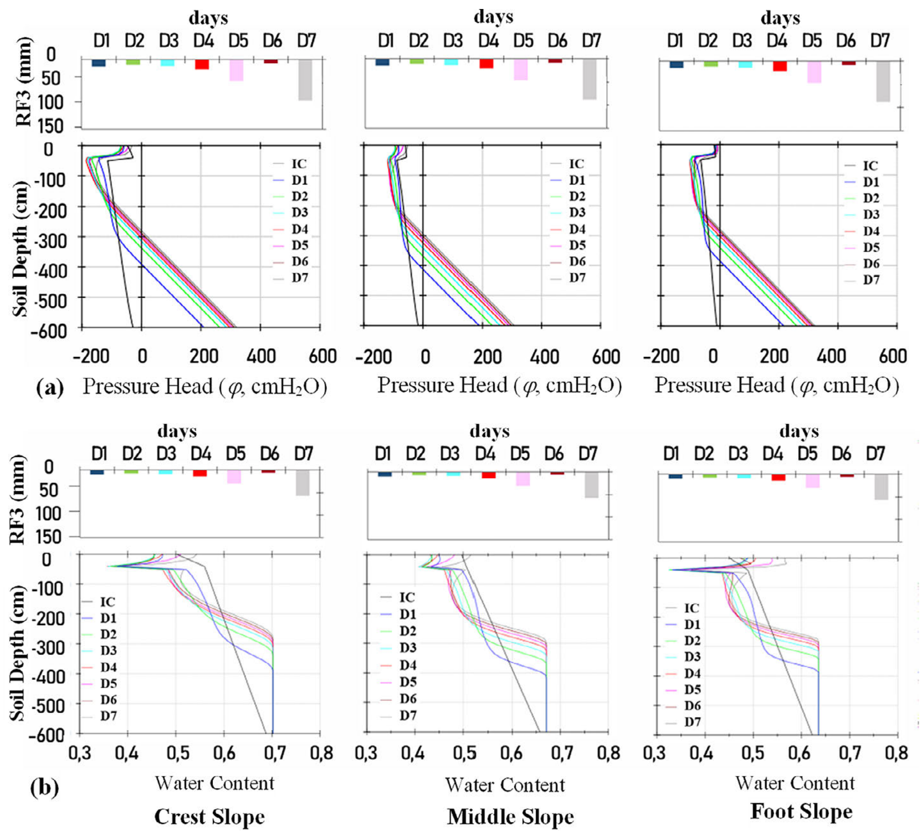

Figure 15. Temporal and vertical distribution of (a) pore water pressure, and (b) water content at the vegetated slope of *Maesopsis eminii* with initial condition pF2 and rainfall of RF3

of *Maessopsis eminii* forest when the (IC) was set up at moist (near saturation) and field capacity conditions (θ at pF1 and pF2) at soil surface and layer –50 cm as shown by black solid lines. The IC and soil hydraulic properties are the same as those on the bare land slopes.

When the RF1 is reduced by canopy interception of *Maessopsis eminii* forests (Fig. 10), the surface layer never reaches saturation condition, and deeper layers reach saturation condition slower than in the bare land slope. The same condition of PWP and θ changes also occur when the rainfall intensities are increased in the 1st and 2nd days (RF2), those are the surface layers that do not reach saturation condition. However, the decreasing PWP and increasing θ in the upper layers are faster than when the rainfall intensity on the 1st and 2nd days is lower (Fig. 12). When the rain intensity was low on the 1st to 6th days (< 50 mm/s) and the rain intensity was high (> 50 mm/day) on the 7th day (RF2), the PWP and θ change were little on the 1st to 6th days and relatively larger on the 7th day (Fig. 13). Dryer IC of θ at pF2 the soil surface never reaches the saturation condition even though the rainfall intensities are high (RF3) as shown in Figure 13–15.

Based on the results of RF1 to RF2 simulations on IC and θ near saturation (pF1) and field capacity (pF2), the effect of tree vegetation canopy interception (*Maesopsis eminii*) of 35% rainfall on PWP and θ changes is very significant. The PWP and θ at the soil surface did not reach saturation conditions, while in the condition of bare soils, PWP and θ at the soil surface reached saturation in the rainfall events RF1, RF2, and RF3. The lower change of PWP in forested slope is also shown by the research of Guo et al. [2024], that the PWP in a forested slope can be up to 1.5 times lower than in a bare slope.

The percentage of rainfall that is intercepted by the tree canopy varies greatly. In temperate forests, canopy interceptions range from 20% to 30% globally, with specific studies showing conifer species intercepting 51.6% to 95.9% of precipitation, while broadleaf species capture 20.1% to 67.7% [De Mello et al., 2024; Fischer et al., 2023]. Deciduous forests in Denmark showed an interception loss of 35%, while coniferous forests had a higher interception loss of 51% [Andreasen et al., 2023], and *Pinus tabulaeformis* plantations in China exhibited a canopy interception rate of

14.7% to 17.9% [Qian et al., 2022]. In tropical natural forests, the interception could reach 53% of rainfall [Diet et al., 2006].

The variation in canopy interception is influenced not only by the vegetation canopy's characteristics, but also by rain events, and rain events also affect the behavior of PWP and θ changes as shown in Figures 10–15. Guo et al. [2024] research shows that the plant efficiently inhibits rainwater penetration and maintains slope stability during short periods of 4 hrs of high rainfall. However, for lengthy periods of 168 hrs of rainfall, the plant's hydrological advantage on slope stability may be insufficient. The mechanical strengthening of the root can still be useful in retaining slope stability.

The changes in PWP and θ in vegetated soils are influenced by various factors: rain that reaches the surface of mineral soils as the effect of canopy interception and root systems. Root systems significantly affect PWP by altering water permeability. Root water uptake influences the PWP, suggesting that an increase in root volume will elevate the (negative) PWP, which is shown by the ratio of transpiration rate to saturated hydraulic conductivity. The negative pressure potential due to root water absorption increases as the total water permeability under the plant layer decreases [Liu et al., 2018].

CONCLUSIONS

Rainfall events and soil hydraulics properties of soil profiles influence the behavior of PWP and θ changes on bare and forested slopes. The soil hydraulic properties of surface layers that cause $K(\varphi)$ to be greater than $K(\varphi)$ in the lower layers result in PWP increase and decrease θ in both the initial conditions of water content (θ) at near saturation (pF1) and field capacity (pF2), including when there is rainfall with an intensity less than $K(\varphi)$, and $K(\varphi)$ of deeper soil layers decreases in line with the θ increasing. The θ increasing from the lower to the upper layers continues as rain occurs continuously. The θ could reach saturation in a soil profile of 6 m depth when the soil is bare. In contrast, when *Maesopsis eminii* covers the soil stand with the capacity of canopy interception of 35% of precipitation, the θ never reaches saturation condition at the surface layers within 7 days of rainfall events with the rainfall intensity is less 121 mm/d and total 282.6 mm/7 days. Low rainfall intensity on the 1st to 6th days (< 50 mm/s) and followed the high rainfall intensity (> 50 mm/day) on the 7th day (RF2), the PWP and θ change were little on the 1st to 6th days and relatively larger on the 7th day.

Acknowledgements

The PMDSU (Master leading to PhD) Program of The Ministry of Education, Culture, Research, and Technology of The Republic of Indonesia partially funded this research. We thank the PMDSU Program Management and the surveyor team who helped in collecting field data.

REFERENCES

1. Andreasen M., Christiansen J.R., Sonnenborg T.O., Stisen S., Looms, M.C. (2023). Seasonal dynamics of canopy interception loss within a deciduous and a coniferous forest. *Hydrological Processes, 37*(4). https://doi.org/10.1002/hyp.14828
2. Agbai W., Kosuowei M. (2022). Influence of land-use systems on hydraulic properties of soils in Yenagoa and Amassoma, Bayelsa State, Nigeria. *International Journal of Environment*. https://doi.org/10.3126/ije.v11i1.45838
3. Anlauf R. (2014). Using the EXCEL solver function to estimate the van Genuchten parameters from measured pF/water content values. Excel spreadsheed retrieved from www.al.hs-osnabrueck.de/anlauf.html on [July 2022]
4. Asdak C., Jarvis P., Van Gardingen P., Fraser, A. (1998). Rainfall interception loss in unlogged and logged forest areas of Central Kalimantan, Indonesia. *Journal of Hydrology, 206*(3–4), 237–244. https://doi.org/10.1016/s0022-1694(98)00108-5
5. Bonell M. (1993). Progress in understanding runoff generation dynamics in forests. *Journal of Hydrology, 150*, 217–275. https://doi.org/10.1016/0022-1694(93)90112-M
6. Brook R.H., Corey A.T. (1964). Hydraulic properties of porous media. Hydrology Papers. Colorado State University
7. Buttle J.M., House D.A. (1997). Spatial variability of saturated hydraulic conductivity in shallow macroporous soils in a forested basin. *Journal of Hydrology, 203*, 127–142
8. Couvreur V., Vanderborght J., Draye X., Javaux M. (2014). Dynamic aspects of soil water availability for isohydric plants: Focus on root hydraulic resistances. *Water Resources Research, 50*, 8891–8906. https://doi.org/10.1002/2014WR015608
9. De Mello C.R., Guo L., Yuan C., Rodrigues A.F.,

Lima R.R., Terra M.C. (2024). Deciphering global patterns of forest canopy rainfall interception (FCRI): A synthesis of geographical, forest species, and methodological influences. *Journal of Environmental Management, 358*, 120879. https://doi.org/10.1016/j.jenvman.2024.120879

10. Dexter A. (1988). Advances in characterization of soil structure. *Soil and Tillage Research, 11*(3–4), 199–238. https://doi.org/10.1016/0167-1987(88)90002-5
11. Dietz J., Hölscher D., Leuschner C., Hendrayanto N. (2006). Rainfall partitioning in relation to forest structure in differently managed montane forest stands in Central Sulawesi, Indonesia. *Forest Ecology and Management, 237*(1–3), 170–178. https://doi.org/10.1016/j.foreco.2006.09.044
12. Dlapa P., Hriník D., Hrabovský A., Šimkovic I., Žarnovičan H., Sekucia F., Kollár, J. (2020). The impact of land-use on the hierarchical pore size distribution and water retention properties in loamy soils. *Water, 12*, 339. https://doi.org/10.3390/w12020339
13. Elfadil, M.E. (2018). Effect of antecedent rainfall on pore-water pressure distribution characteristics in residual soil slopes under tropical rainfall. *International Journal of Hydrology*. https://doi.org/10.15406/ijh.2018.02.00152
14. El-Ghany B.F., Arafa R.A.M., El-Rahmany T.A., El-Shazly M.M. (2010). Effect of some soil microorganisms on soil properties and wheat production under North Sinai conditions. *Journal of Applied Sciences Research. 6*, 559–579.
15. Fata Y.A., Hendrayanto, Erizal, Tarigan S.D. (2021). 2D and 3D Ground Model Development for Mountainous Landslide Investigation. IOP Conf. Series: Earth and Environmental Science, 1–12. https://doi.org/10.1088/1755-1315/871/1/012057
16. Fata Y.A., Hendrayanto, Pratama Y., Suria D. (2023). Evaluation of the gash rainfall interception model in forest plantations. *Journal of Hunan University Natural Sciences, 50*(12). https://doi.org/10.55463/issn.1674-2974.50.12.3
17. Fischer D.G., Vieira S.T., Jayakaran A.D. (2023). Distinct rainfall interception profiles among four common pacific northwest tree species. *Forests, 14*(1), 144. https://doi.org/10.3390/f14010144
18. Gonzalez-Ollauri A., Mickovski S.B. (2017). Hydrological effect of vegetation against rainfall-induced landslides. *Journal of Hydrology, 549*, 374–387. https://doi.org/10.1016/j.jhydrol.2017.04.014
19. Guan N., Cheng J., Shi X. (2023). Preferential flow and preferential path characteristics of the typical forests in the Karst Region of Southwest China. *Forests, 14*(6), 1248. https://doi.org/10.3390/f14061248
20. Guo H., Ng C.W.W., Zhang Q. (2024). Three-dimensional numerical analysis of plant-soil hydraulic interactions on pore water pressure of vegetated slope under different rainfall patterns. *Journal of Rock Mechanics and Geotechnical Engineering, 16*(9), 3696–3706. https://doi.org/10.1016/j.jrmge.2023.09.032
21. Hemid E.M., Kántor T., Tamma A.A., Masoud M.A. (2021). Effect of groundwater fluctuation, construction, and retaining system on slope stability of Avas Hill in Hungary. Open Geosciences, 13, 1139–1157. https://doi.org/10.1515/geo-2020-0294
22. Hendrayanto, Kosugi K.T.U., Sakiki M., Mizuyama T. (1999). Spatial variability of soil hydraulic properties in a forested hillslope. *J. For. Res, 4*, 107–114
23. Hendrayanto, Kosugi K., Mizuyama T. (2000). Scaling hydraulic properties of forest soils. *Hydrological Process, 14*, 521–538.
24. Hendrickx M.G., Diels J., Janssens P., Schlüter S., Vanderborght J. (2023). Temporal covariance of spatial soil moisture variations: A mechanistic error modeling approach. *Vadose Zone Journal, 23*. https://doi.org/10.1002/vzj2.20295
25. Ibrahim A., Mukhlisin M., Jaafar O. (2013). Numerical Assessment of Rainfall Infiltration into Soil Column for the Unsaturated Layered Residual Forest Soil. *Jurnal Teknologi, 65*(2), 121–127. https://doi.org/10.11113/jt.v65.2200
26. Jabro J.D., Stevens W.B. (2022). Pore size distribution derived from soil–water retention characteristic curve as affected by tillage intensity. *Water, 14*(21), 3517. https://doi.org/10.3390/w14213517
27. Kharel G., Dhakal M., Deb S.K., Slaughter L.C., Simpson C., West C.P. (2023). Effect of long-term semiarid pasture management on soil hydraulic and thermal properties. *Plants, 12*(7), 1491. https://doi.org/10.3390/plants12071491
28. Kosugi K. (1996). Lognormal distribution model for unsaturated soil hydraulic properties. *Water Resour. Res., 32*(9), 2697–2703.
29. Kosugi K. (1997). Effect of pore radius distribution of forest soils on vertical water movement in soil profile. *Journal of Japan Society of Hydrology & Water Resources, 10*, 226–237.
30. Kuti'lek M., Nielsen D.R. (1994). Soil Hydrology. Catena Verlag, 104–105, Cremlingen, Germany.
31. Li Y., Liang Y., Wei T., Chen P., Ji X., Liu X. (2023). Spatiotemporal dynamics of rainfall interception and effective precipitation in the Loess Plateau after large-scale afforestation. *Land Degradation & Development, 34*, 5004 – 5016. https://doi.org/10.1002/ldr.4825
32. Liu H., Feng S., Garg A., Ng C. (2018). Analytical solutions of pore-water pressure distributions in a vegetated multi-layered slope considering the effects of roots on water permeability. *Computers and Geotechnics, 102*, 252–261. https://doi.org/10.1016/j.compgeo.2018.06.003

33. Maturidi A.M.A.M., Kasim N., Taib K.A., Azahar W.N.A.W. (2021). Rainfall-Induced landslide thresholds development by considering different rainfall parameters: A review. *Journal of Ecological Engineering, 22*(10), 85–97. https://doi.org/10.12911/22998993/142183
34. Móricz N., Mátyás C., Berki I., Rasztovits E., Vekerdy Z., Gribovski Z. (2012). Comparative water balance study of forest and fallow plots. *iForest, 5*, 188–196. https://doi.org/10.3832/ifor0624-005
35. Mualem Y. (1976). A new model for predicting the hydraulic conductivity of unsaturated porous media. *Water Resour. Res., 12*(3), 513–522.
36. Noguchi S., Tsuboyama Y., Sidle R.C., Hosoda I. (1997). Spatially distributed morphological characteristics of macropores in forest soils of Hitachi Ohta Experimental Watershed, Japan. *Journal of Forest Research, 2*, 207–215.
37. Podhrázská J., Kučera J., Karásek P., Szturc J., Konečná J. (2021). The effect of land management on the retention capacity of agricultural land in the conditions of climate change – case study. *Journal of Ecological Engineering, 22*(1), 258–266. https://doi.org/10.12911/22998993/130230
38. Prado Hernández J.V., Pascual Ramírez F., Martínez Ruiz A., Cristóbal A.D. (2023). Surface water balance at the Chapingo River basin: rainfall intercepted by vegetation and water infiltration into the soil. *Agro Productividad*. https://doi.org/10.32854/agrop.v16i9.2586
39. Proteau A., Guittonny M., Bussière B. (2023). Impact of roots on the hydrogeological properties of silty soil covers. *Canadian Geotechnical Journal*. https://doi.org/10.1139/cgj-2023-0016
40. Qian Y., Shi C., Zhao T., Lu J., Bi B., Luo G. (2022). Canopy interception of different rainfall patterns in the rocky mountain areas of Northern China: An application of the revised gash model. *Forests, 13*(10), 1666. https://doi.org/10.3390/f13101666
41. Rashid N.S.A., Askari M., Tanaka T., Simunek J., van Genuchten M.T. (2015). Inverse estimation of soil hydraulic properties under oil palm trees. *Geoderma*, 241–242, 306–312. https://doi.org/10.1016/j.geoderma.2014.12.003
42. Rashid N.S., Askari M. (2014). "Litter marks" around oil palm tree base indicating infiltration area of stemflow-induced water. *National Seminar on Civil Engineering Research*, 14–15 April, 2014, Johor Bahru, Malaysia
43. Salee R., Chinkulkijniwat A., Yubonchit S., Van D.B. (2022). Rainfall threshold for landslide warning in southern thailand –an integrated landslide susceptibility map with rainfall event –duration threshold. *Journal of Ecological Engineering, 23*(12), 124–133. https://doi.org/10.12911/22998993/155023
44. Sidle C.R., Ziegler A.D. (2017). The canopy interception–landslide initiation conundrum: insight from a tropical secondary forest in northern Thailand. *Hydrology Earth System Science, 21*, 651–667. https://doi.org/10.5194/hess-21-651-2017
45. Simunek J., Sejna M., Saito H., Sakai M., Van Genuchten M.T.H. (2013). The HYDRUS-1D software package for simulating the one-dimensional movement of water. *Heat and Multiple Solutes in Variably-Saturated Media Version 4*, 17, 1–343. California: University of California Riverside.
46. Suryatmojo H., Imron M.A. (2017). Hydrological processes in different types of teak (*Tectona grandis* L.) *Plantation*. In Springer eBooks, 11–19. https://doi.org/10.1007/978-981-10-5430-3_2
47. Tárník A., Igaz D. (2020). Spatial scale analysis of soil water content in agricultural soils of the Nitra River Catchment (Slovakia). *Journal of Ecological Engineering, 21*(1), 112–119. https://doi.org/10.12911/22998993/113076
48. Terzaghi K. (1923). Die Berechnung der Durchlassigkeitsziffer des Tones aus Dem Verlauf der Hidrodynamichen Span-Nungserscheinungen, Akademie der Wissenschaften in Wien, Mathematish-Naturwissen-SchaftilicheKlasse: Mainz, Germany, 125–138.
49. Tian W., Peiffer H., Malengier B., Xue S., Chen Z. (2022). Slope stability analysis method of unsaturated soil slopes considering pore gas pressure caused by rainfall infiltration. *Applied Sciences, 12*(21), 11060. https://doi.org/10.3390/app122111060
50. Van Genuchten M.T.H. (1980). A closed-form equation for predicting the hydraulic conductivity of unsaturated soils. *Soil Science Society of America Journal, 44*, 892–898. doi:10.2136/sssaj1980.03615995004400050002x
51. Virano-Riquelme V., Feger K., Julich S. (2022). Variation in hydraulic properties of forest soils in temperate climate zones. Forests, 13(11), 1850, https://doi.org/10.3390/f13111850
52. Wu T.H., McKinnell III W.P., Swanston D.N. (1979). Strength of tree roots and landslides on Prince of Wales Island, Alaska. *Can Geotech J., 16*(1), 19–33. https://doi.org/10.1139/t79-003
53. Yu M., Zhang L., Xu X., Feger K., Wang Y., Liu W., Schwärzel K. (2015). Impact of land-use changes on soil hydraulic properties of calcaric regosols on the loess plateau, NW China. Journal of Plant Nutrition and Soil Science, 178, 486–498. https://doi.org/10.1002/jpln.201400090
54. Zhong, F., Martens, B., van Dijk, A., Ren, L., Jiang, S., and Miralles, D.G. (2020). Global estimates of rainfall interception loss from satellite observations: recent advances in GLEAM, EGU General Assembly 2020, Online, 4–8 May 2020, EGU2020-13975. https://doi.org/10.5194/egusphere-egu2020-13975